Low temperature X-ray absorption spectroscopy study of $CuMoO_4$ and $CuMo_{0.90}W_{0.10}O_4$ using reverse Monte-Carlo method

Inga Jonane[a,*], Arturs Cintins[a], Aleksandr Kalinko[b], Roman Chernikov[c], Alexei Kuzmin[a]

[a]*Institute of Solid State Physics, University of Latvia, Kengaraga street 8, LV-1063 Riga, Latvia*
[b]*Universität Paderborn, Naturwissenschaftliche Fakultät, Department Chemie, Warburger Strasse 100, 33098 Paderborn, Germany*
[c]*DESY Photon Science, Notkestraße 85, D-22607 Hamburg, Germany*

Abstract

Reversible thermochromic phase transition between α- and γ-phases was studied in $CuMoO_4$ and $CuMo_{0.90}W_{0.10}O_4$ using X-ray absorption spectroscopy in the temperature range of 10–300 K. Reverse Monte Carlo modelling with evolutionary algorithm approach at several absorption edges simultaneously was applied to extract structural information encoded in the experimental EXAFS spectra. The obtained results show that an addition of 10 mol% of tungsten to $CuMoO_4$ induces local distortions in the structure and stabilizes the γ-phase, leading to an increase of the phase transition temperature by ~50-100 K.

Keywords: $CuMoO_4$, X-ray absorption spectroscopy, EXAFS, XANES, reverse Monte Carlo

*Corresponding author
E-mail address:* inga.jonane@cfi.lu.lv (Inga Jonane).

1. Introduction

Copper molybdate ($CuMoO_4$) exhibits thermochromism and piezochromism (Wiesmann et al. (1997)) originated from the first-order structural phase transition accompanied with a drastic colour change between green and brownish-red. While both phases have triclinic $P\bar{1}$ symmetry, the crystal structure of γ-$CuMoO_4$ is built up of distorted CuO_6 and MoO_6 octahedra, whereas the structure of α-$CuMoO_4$ is composed of distorted CuO_6 octahedra, CuO_5 square-pyramids and MoO_4 tetrahedra. According to the pressure-temperature phase diagram (Wiesmann et al. (1997)), α-to-γ phase transition takes place during cooling below ~200 K or at room temperature (RT) by applying ~0.2 GPa pressure. Furthermore, the phase transition temperature can be increased by inducing chemical pressure upon substitution of molybdenum ions with tungsten ones (Gaudon et al. (2007a)). Depending on the tungsten concentration in $CuMo_{1-x}W_xO_4$ solid solutions, phases isostructural to high pressure $CuMoO_4$ can be obtained (Wiesmann et al. (1997); Yanase et al. (2013); Benchikhi et al. (2017)).

The most attractive for technological applications compound in the solid solution series is $CuMo_{0.90}W_{0.10}O_4$, because of its ability to switch between the two allotropic forms (α and γ) in the temperature range from 0 to 100 °C (Gaudon et al. (2007a); Yanase et al. (2013); Robertson et al. (2015); Blanco-Gutierrez et al. (2015)). It was shown (Gaudon et al. (2007b)) that a pressure induced by a finger is enough to promote α-to-γ phase transition in $CuMo_{0.90}W_{0.10}O_4$ at RT. The compound exhibits also halochromic properties, i.e. colour change upon solution pH variation, induced by surface protonation (Gaudon et al. (2010)). A pronounced thermosalient ("jumping crystals") effect caused by the phase transition has been also observed in $CuMo_{0.90}W_{0.10}O_4$ (Robertson et al. (2015)).

In order to better understand the structure-property relationships in $CuMo_{1-x}W_xO_4$, we performed temperature-dependent X-ray absorption spectroscopy (XAS) studies. We have shown recently (Jonane et al. (2018c)) that a variation of the X-ray absorption near edge structure (XANES) at the Mo K-edge in $CuMoO_4$ correlates with a degree of the molybdenum–oxygen coordination polyhedra distortion, both showing the hysteretic behavior upon α-to-γ phase transition (Fig. 1).

113
114
115
116
117
118
119
120
121
122
123
124
125
126
127
128
129
130
131
132
133
134
135
136
137
138
139
140
141
142
143
144
145
146
147
148
149
150
151
152
153
154
155
156
157
158
159
160
161
162
163
164
165
166
167
168

Extended X-ray absorption fine structure (EXAFS) data analysis of $CuMoO_4$ and $CuMo_{0.90}W_{0.10}O_4$ is challenging task due to the low symmetry of the α and γ phases, leading to a distortion of the local environment. In such case, the conventional EXAFS analysis is less effective because of a large number of fitting parameters required. Previously, we have employed a regularization-like method to reconstruct the radial distribution functions (RDFs) within the first coordination shell of Mo atoms in $CuMoO_4$ (Jonane et al. (2018b)). Here we extend our analysis beyond the first shell using advanced reverse Monte-Carlo (RMC) calculations based on evolutionary algorithm (Timoshenko et al. (2014c)) at several absorption edges simultaneously. We compare pure $CuMoO_4$ and $CuMo_{0.90}W_{0.10}O_4$ with the aim to understand the role of tungsten in the functional properties of $CuMo_{1-x}W_xO_4$ solid solutions.

2. Experimental

Polycrystalline $CuMoO_4$ powder was synthesized using solid-state reaction method by heating a mixture of CuO and MoO_3 powders at 650 °C in air for 8 hours followed by cooling down naturally to room temperature. The same synthesis method was applied for $CuMo_{0.90}W_{0.10}O_4$ by adding stoichiometric amount of WO_3. The as-prepared green powders had α-phase, confirmed by X-ray diffraction.

Temperature-dependent XAS experiments were conducted at the HASYLAB/DESY PETRA-III P65 undulator beamline. The storage ring was operated at E=6.08 GeV and current I=95 mA in top-up 40 bunch mode. The X-ray absorption spectra were collected at the Cu (8979 eV) and Mo (20000 eV) K-edges and W (10207 eV) L_3-edge during heating and cooling in transmission mode using two ionization chambers. Fixed exit Si(311) double-crystal monochromator was used in experimental set-up, and harmonic rejection was achieved by a coated silicon plane mirror. The Oxford Instruments liquid helium flow cryostat was used to maintain the sample temperature in the range of 10-300 K. The powder samples for XAS measurements were deposited on Millipore filters. The XAS experiment was performed starting at 300 K, next cooling down to 10 K, following by heating up to 300 K, again cooling down to 50 K and finally heating back to 300 K (Fig. 2).

3

3. Reverse Monte Carlo calculations

The experimental EXAFS spectra were analysed using the RMC method based on evolutionary algorithm (EA), as implemented in the EvAX code (Timoshenko et al. (2014c)). The details of the RMC method were reported by us previously and can be found in (Timoshenko et al. (2012)). The method was successfully used for interpretation of EXAFS spectra of numerous materials (Timoshenko et al. (2014a,b); Kalinko et al. (2016); Jonane et al. (2016); Timoshenko et al. (2017); Jonane et al. (2018a)).

Starting structure models of $CuMoO_4$ corresponding to the α and γ phases were constructed based on the diffraction data (Wiesmann et al. (1997)). The model for $CuMo_{0.90}W_{0.10}O_4$ was created by randomly substituting Mo atoms with W atoms in α-$CuMoO_4$ and γ-$CuMoO_4$ structures keeping the stoichiometric ratio of the elements. Several random substitutions were tested. Note that in our RMC method all coordination numbers correspond to that from the diffraction since average crystallographic structure is the starting point of the RMC procedure, and only small displacements of atoms, simulating thermal vibrations, are allowed during the RMC fit.

The RMC calculations were performed using periodic boundary conditions for $4a_0 \times 4b_0 \times 4c_0$ (a_0, b_0 and c_0 are the lattice parameters) large supercell, containing 2304 atoms. All atoms in the supercell were randomly displaced at each RMC iteration with the maximum allowed displacement of 0.4 Å. The configuration-averaged EXAFS spectra at the Cu and Mo K-edges and additionally at the W L_3-edge for $CuMo_{0.90}W_{0.10}O_4$ were calculated using the ab initio self-consistent real-space multiple-scattering (MS) FEFF8.5L code (Ankudinov et al. (1998)) taking into account MS contributions up to the 6th order. The complex energy-dependent exchange-correlation Hedin-Lundqvist potential (Hedin and Lundqvist (1971)) was employed to account for inelastic effects. The amplitude scaling parameter S_0^2=1 was used in all simulations. Comparison between the experimental and theoretical EXAFS spectra was performed in direct (R) and reciprocal (k) space simultaneously using the Morlet wavelet transform (Timoshenko and Kuzmin (2009)). The convergence of RMC simulations was achieved after several thousand of iterations.

The RMC calculations of the experimental data close to γ-to-α phase transition

temperature were performed using the structure models for both phases. The obtained fits for $CuMoO_4$ and $CuMo_{0.90}W_{0.10}O_4$ at selected temperatures are shown in Fig. 3 and 4, respectively. The final atomic configurations were used to calculate the partial RDFs $g(R)$ for further analysis.

4. Results and discussion

The linear combination analysis (LCA) of the Mo K-edge XANES performed in the temperature range from 10 to 300 K, as described in Jonane et al. (2018c), indicates that the phase transition hysteresis in $CuMo_{0.90}W_{0.10}O_4$ is shifted to higher temperatures (Fig. 1) in agreement with previous studies (Gaudon et al. (2007a,b); Yanase et al. (2013)). The transition from α to γ phase occurred between 250 and 100 K upon cooling, whereas the transition from γ to α phase started at about 280 K upon heating and was still not finished at room temperature even several hours after. Optical, calorimetry and magnetic measurement experiments showed that the γ-to-α phase transition in $CuMo_{0.90}W_{0.10}O_4$ occurs during heating in the temperature range between 340 and 380 K (Gaudon et al. (2007a)).

Temperature-dependent EXAFS spectra of $CuMoO_4$ and $CuMo_{0.90}W_{0.10}O_4$ are shown in Fig. 2. One can see that the Cu K-edge spectra are weakly affected during heating from 10 K to 300 K, however some changes occur at 250 K and can be attributed to the transition from CuO_6 octahedra to CuO_5 square-pyramids. The Mo K-edge is drastically affected during the phase transition because molybdenum coordination changes from octahedral to tetrahedral. Finally, it seems that the local environment of tunsgten atoms does not change significantly during the whole cooling and heating experiments.

More detailed analysis can be performed based on the results of RMC calculations reported in Fig. 3 for $CuMoO_4$ and in Fig. 4 for $CuMo_{0.90}W_{0.10}O_4$. Note that the RMC models agree well with the EXAFS spectra at two or three absorption edges, which is crucial for accurate reconstruction of crystal structure for multi-atom compounds (Timoshenko et al. (2014a)).

The experimental EXAFS spectra of $CuMoO_4$ at T=200 and 300 K (Fig. 3) are well described by the structure models of γ and α phases, respectively. At the same

time, the structure models of both α and γ phases give reasonable agreement with the experimental data at T=250 K, indicating coexistence of the two phases in close ratio. This conclusion agrees with the LCA results suggesting the presence of the 60% and 40% of γ and α phases, respectively (Jonane et al. (2018b)).

The results of RMC calculations using α and γ phase structures for $CuMo_{0.90}W_{0.10}O_4$ are shown in Fig. 4. At T=50 K, the EXAFS spectra at the Cu, Mo and W absorption edges are well reproduced using the γ-phase structure model. At the same time, at T=300 K (before cooling), the α-phase model gives good agreement at the Cu and Mo K-edges, but slightly worse agreement at the W L_3-edge, indicating that some relaxation of the local environment around tungsten ions occurs. Indeed, the W L_3-edge EXAFS can be slightly better described by the γ-phase structure, which does not apply to the other two edges. This means that in spite of the crystal lattice of $CuMo_{0.90}W_{0.10}O_4$ at T=300 K (before cooling) corresponds to that in the α-phase, the local structure around W atoms relaxes in an attempt to reconstruct distorted octahedral coordination.

The partial RDFs for Cu–O, Mo–O and W–O atom pairs, calculated from the atom coordinates of the RMC models of $CuMoO_4$ and $CuMo_{0.90}W_{0.10}O_4$, are compared in Fig. 5. Note that the reported RDFs are averaged over all atoms of the same type within the supercell. However, one can also distinguish three non-equivalent crystallographic sites of Cu and Mo atoms with different local environment in $CuMoO_4$.

Further we will consider the nearest groups of oxygen atoms located around metal ions at the distances up to about 3.5 Å. One can see that the Cu and Mo environments are close in both $CuMoO_4$ and $CuMo_{0.90}W_{0.10}O_4$ compounds. At the same time, while the Cu environment is quite similar also at low (50 K) and high (300 K) temperatures, the distributions of the Mo–O atom pairs differ significantly already for the closest 4 oxygen atoms. The tetrahedral coordination in α-phase is more ordered than the octahedral one in γ-phase. In fact, the MoO_6 octahedra are strongly distorted with a distribution of the Mo–O distances from ~1.5 Å to ~2.8 Å. The group of four nearest oxygen atoms is responsible for a sharp peak in the RDFs at ~1.8 Å. These results are in agreement with those obtained by the regularization-like method (Jonane et al. (2018b)).

Next, we compare the W–O and Mo–O distributions in $CuMo_{0.90}W_{0.10}O_4$ to un-

derstand how large is the local structure relaxation around tungsten atoms. At low temperature (50 K) in γ-phase, tungsten atoms have distorted octahedral coordination close to that of molybdenum (Fig. 5(E)). The distortion of WO_6 and MoO_6 octahedra is due to the second-order Jahn–Teller effect (Kunz and Brown (1995)) caused by the charge transfer from oxygen atoms surrounding metal ion, having formally 6+ oxidation state ($5d^0$ electron configuration). At T=300 K in α-phase, when the coordination of molybdenum atoms becomes tetrahedral, tungsten atoms tend to have more distorted environment (Fig. 5(F)): there is an additional group of oxygen atoms at about 2.1 Å, and the next group of oxygen atoms at 2.8 Å is slightly displaced and split. Moreover, the RMC calculations at the W L_3-edge for α-$CuMo_{0.90}W_{0.10}O_4$ using the structure model corresponding to γ-phase (W in distorted octahedral environment) give slightly better agreement with the experiment, however, the shape of the W–O distribution is quite similar to that in the α-phase.

To conclude, our results confirm the tendency of tungsten atoms in $CuMo_{0.90}W_{0.10}O_4$ to adapt distorted octahedral environment when substituting molybdenum atoms, thus affecting the temperature/pressure of α-to-γ phase transition and helping to stabilize γ-phase at room temperature.

5. Conclusions

X-ray absorption spectroscopy was used to probe a variation of the local atomic structure in $CuMoO_4$ and $CuMo_{0.90}W_{0.10}O_4$ in the temperature range of 10-300 K. Advanced data analysis of EXAFS spectra at several absorption edges simultaneously interpreted by reverse Monte Carlo method allowed us to monitor the α-to-γ and γ-to-α thermochromic phase transitions, occuring gradually with the two phase coexistence range. We observed that the addition of 10 mol% of tungsten to $CuMoO_4$ induces local distortions and stabilizes the γ-phase, leading to an increase of the phase transition temperature by ~50-100 K.

Acknowledgements

References

Ankudinov, A.L., Ravel, B., Rehr, J.J., Conradson, S.D., 1998. Real-space multiple-scattering calculation and interpretation of X-ray-absorption near-edge structure. Phys. Rev. B 58, 7565–7576. doi:10.1103/PhysRevB.58.7565.

Benchikhi, M., El Ouatib, R., Guillemet-Fritsch, S., Er-Rakho, L., Durand, B., 2017. Investigation of structural transition in molybdates $CuMo_{1-x}W_xO_4$ prepared by polymeric precursor method. Process. Appl. Ceram. 11, 21–26. doi:10.2298/PAC1701021B.

Blanco-Gutierrez, V., Cornu, L., Demourgues, A., Gaudon, M., 2015. $CoMoO_4/CuMo_{0.9}W_{0.1}O_4$ mixture as an efficient piezochromic sensor to detect temperature/pressure shock parameters. ACS Appl. Mater. Interfaces. 7, 7112–7117. doi:10.1021/am508652h.

Gaudon, M., Carbonera, C., Thiry, A.E., Demourgues, A., Deniard, P., Payen, C., Létard, J.F., Jobic, S., 2007a. Adaptable thermochromism in the $CuMo_{1-x}W_xO_4$ series ($0 \leq x < 0.1$): A behavior related to a first-order phase transition with a transition temperature depending on x. Inorg. Chem. 46, 10200–10207. doi:10.1021/ic701263c.

Gaudon, M., Deniard, P., Demourgues, A., Thiry, A.E., Carbonera, C., Le Nestour, A., Largeteau, A., Létard, J.F., Jobic, S., 2007b. Unprecedented "one-finger-push"-induced phase transition with a drastic color change in an inorganic material. Adv. Mater. 19, 3517–3519. doi:10.1002/adma.200700905.

449
450
451
452
453
454
455

Gaudon, M., Riml, C., Turpain, A., Labrugere, C., Delville, M.H., 2010. Investigation of the chromic phase transition of $CuMo_{0.9}W_{0.1}O_4$ induced by surface protonation. Chem. Mater. 22, 5905–5911. doi:`10.1021/cm101824d`.

Hedin, L., Lundqvist, B.I., 1971. Explicit local exchange-correlation potentials. J. Phys. C: Solid State Phys. 4, 2064–2083. doi:`10.1088/0022-3719/4/14/022`.

Jonane, I., Anspoks, A., Kuzmin, A., 2018a. Advanced approach to the local structure reconstruction and theory validation on the example of the W L_3-edge extended X-ray absorption fine structure of tungsten. Modelling Simul. Mater. Sci. Eng. 26, 025004. doi:`10.1088/1361-651X/aa9bab`.

Jonane, I., Cintins, A., Kalinko, A., Chernikov, R., Kuzmin, A., 2018b. Probing the thermochromic phase transition in $CuMoO_4$ by EXAFS spectroscopy. Phys. Status Solidi B 255, 1800074. doi:`10.1002/pssb.201800074`.

Jonane, I., Cintins, A., Kalinko, A., Chernikov, R., Kuzmin, A., 2018c. X-ray absorption spectroscopy of thermochromic phase transition in $CuMoO_4$. Low Temp. Phys. 44, 434–437. doi:`10.1063/1.5034155`.

Jonane, I., Lazdins, K., Timoshenko, J., Kuzmin, A., Purans, J., Vladimirov, P., Gräning, T., Hoffmann, J., 2016. Temperature-dependent EXAFS study of the local structure and lattice dynamics in cubic Y_2O_3. J. Synchrotron Rad. 23, 510–518. doi:`10.1107/S1600577516001181`.

Kalinko, A., Bauer, M., Timoshenko, J., Kuzmin, A., 2016. Molecular dynamics and reverse Monte Carlo modeling of scheelite-type AWO_4 (A= Ca, Sr, Ba) W L_3-edge EXAFS spectra. Phys. Scr. 91, 114001. doi:`10.1088/0031-8949/91/11/114001`.

Kunz, M., Brown, I., 1995. Out-of-center distortions around octahedrally coordinated d^0 transition metals. J. Solid State Chem. 115, 395–406. doi:`10.1006/jssc.1995.1150`.

Robertson, L., Penin, N., Blanco-Gutierrez, V., Sheptyakov, D., Demourgues, A., Gaudon, M., 2015. $CuMo_{0.9}W_{0.1}O_4$ phase transition with thermochromic,

9

504

piezochromic, and thermosalient effects. J. Mater. Chem. C 3, 2918–2924. doi:10.1039/C4TC02463J.

Timoshenko, J., Anspoks, A., Kalinko, A., Kuzmin, A., 2014a. Analysis of extended x-ray absorption fine structure data from copper tungstate by the reverse Monte Carlo method. Phys. Scr. 89, 044006. doi:10.1088/0031-8949/89/04/044006.

Timoshenko, J., Anspoks, A., Kalinko, A., Kuzmin, A., 2014b. Temperature dependence of the local structure and lattice dynamics of wurtzite-type ZnO. Acta Mater. 79, 194–202. doi:10.1016/j.actamat.2014.07.029.

Timoshenko, J., Anspoks, A., Kalinko, A., Kuzmin, A., 2017. Thermal disorder and correlation effects in anti-perovskite-type copper nitride. Acta Mater. 129, 61–71. doi:10.1016/j.actamat.2017.02.074.

Timoshenko, J., Kuzmin, A., 2009. Wavelet data analysis of EXAFS spectra. Comp. Phys. Commun. 180, 920–925. doi:10.1016/j.cpc.2008.12.020.

Timoshenko, J., Kuzmin, A., Purans, J., 2012. Reverse Monte Carlo modeling of thermal disorder in crystalline materials from EXAFS spectra. Comp. Phys. Commun. 183, 1237–1245. doi:10.1016/j.cpc.2012.02.002.

Timoshenko, J., Kuzmin, A., Purans, J., 2014c. EXAFS study of hydrogen intercalation into ReO_3 using the evolutionary algorithm. J. Phys.: Condens. Matter 26, 055401. doi:10.1088/0953-8984/26/5/055401.

Wiesmann, M., Ehrenberg, H., Miehe, G., Peun, T., Weitzel, H., Fuess, H., 1997. *p-T* phase diagram of $CuMoO_4$. J. Solid State Chem. 132, 88–97. doi:10.1006/jssc.1997.7413.

Yanase, I., Mizuno, T., Kobayashi, H., 2013. Structural phase transition and thermochromic behavior of synthesized W-substituted $CuMoO_4$. Ceram. Int. 39, 2059–2064. doi:10.1016/j.ceramint.2012.08.059.

561
562
563
564
565
566
567
568
569
570
571
572
573
574
575
576
577
578
579
580
581
582
583
584
585
586
587
588
589
590
591
592
593
594
595
596
597
598
599
600
601
602
603
604
605
606
607
608
609
610
611
612
613
614
615
616
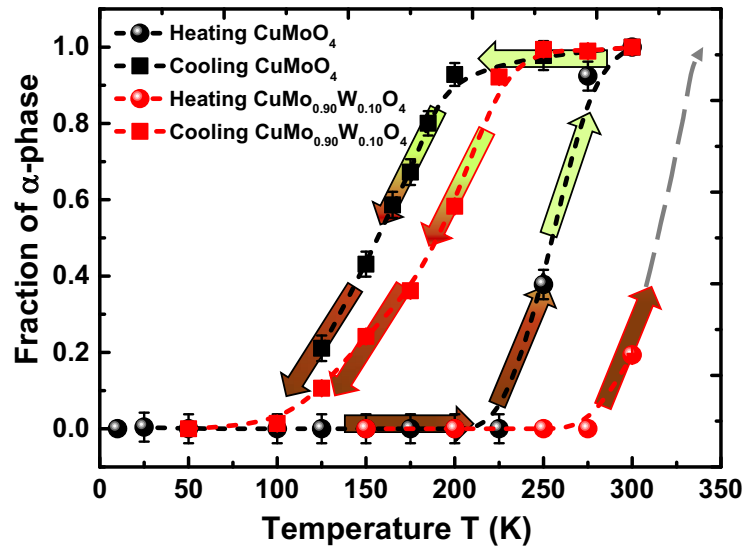

Figure 1: Temperature dependence of the fraction of α phase in $CuMoO_4$ and $CuMo_{0.90}W_{0.10}O_4$ samples upon heating and cooling. Gray dashed arrow is an extrapolation above the room temperature for $CuMo_{0.90}W_{0.10}O_4$.
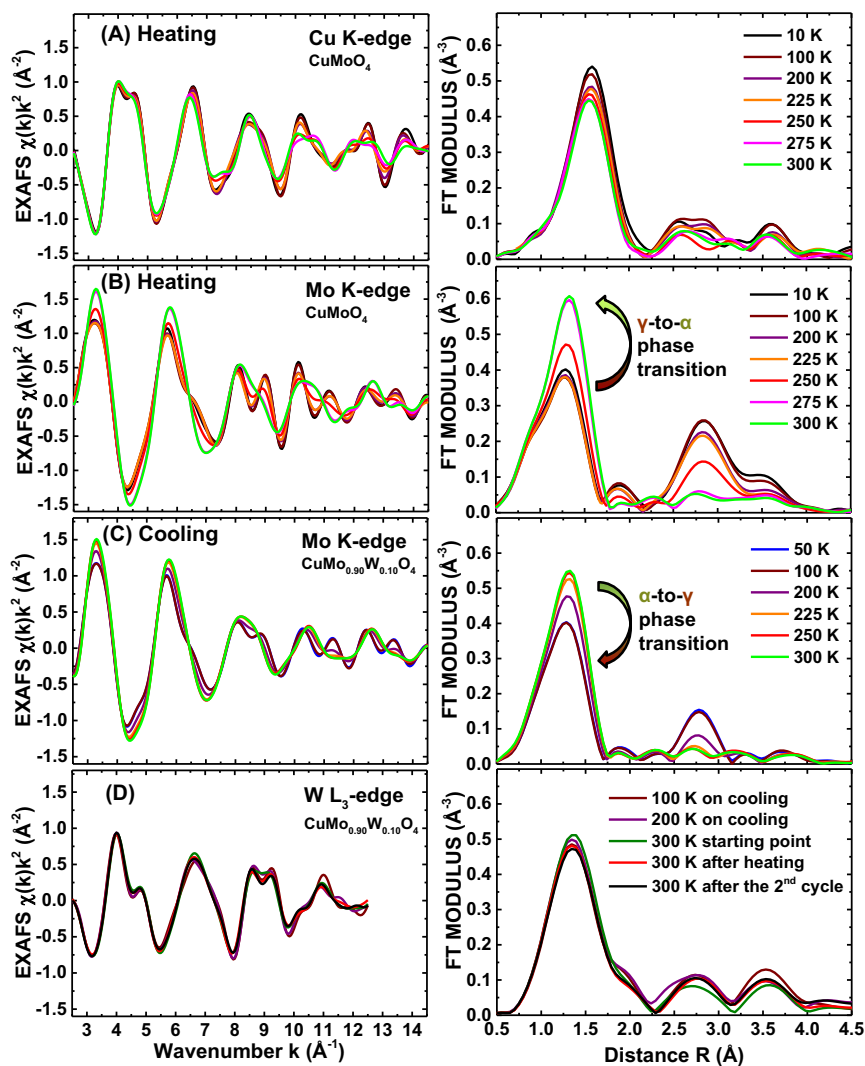
Figure 2: Temperature-dependence of the experimental EXAFS spectra $\chi(k)k^2$ and their Fourier transforms (FTs) for the Cu (A) and Mo (B) K-edges in $CuMoO_4$ during heating from 10 K to 300 K, for the Mo K-edge (C) in $CuMo_{0.90}W_{0.10}O_4$ during cooling from 300 K to 50 K and for the W L_3-edge (D) in $CuMo_{0.90}W_{0.10}O_4$ at different stages of the experiment.

12

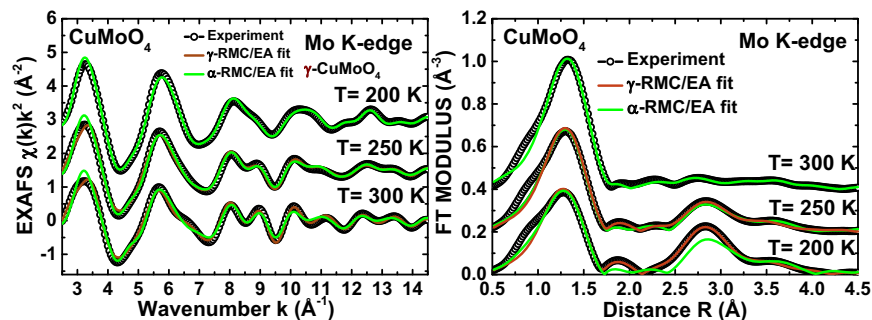Figure 3: Results of RMC calculations for the Mo K-edge in $CuMoO_4$ at selected temperatures. Left panel: the experimental and calculated EXAFS spectra $\chi(k)k^2$ using α- and γ-$CuMoO_4$ initial structure models. Right panel: the corresponding Fourier transforms.
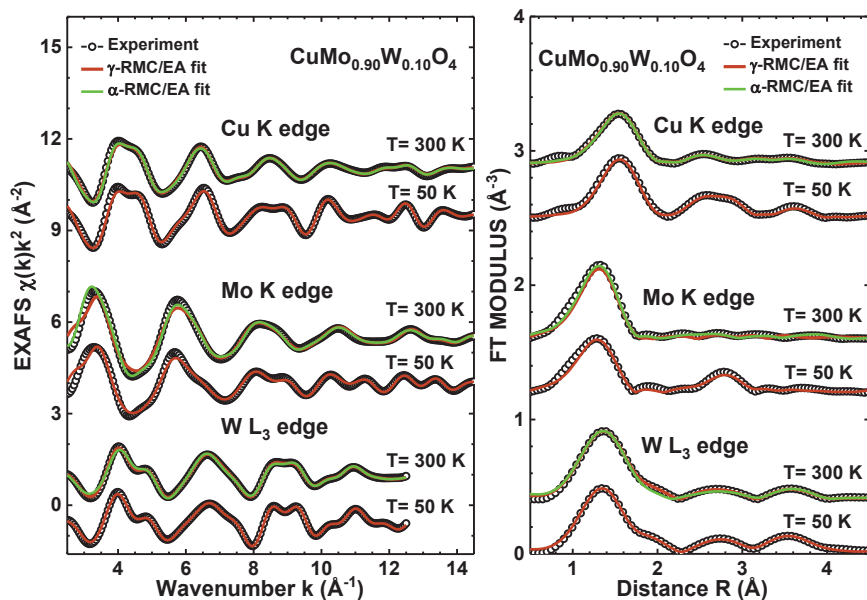

Figure 4: Results of RMC calculations for the Cu K-edge, Mo K-edge and W L_3-edge in $CuMo_{0.90}W_{0.10}O_4$ at $T=50$ K (γ-phase) and $T=300$ K (α-phase). Left panel: the experimental and calculated EXAFS spectra $\chi(k)k^2$. Right panel: the corresponding Fourier transforms.
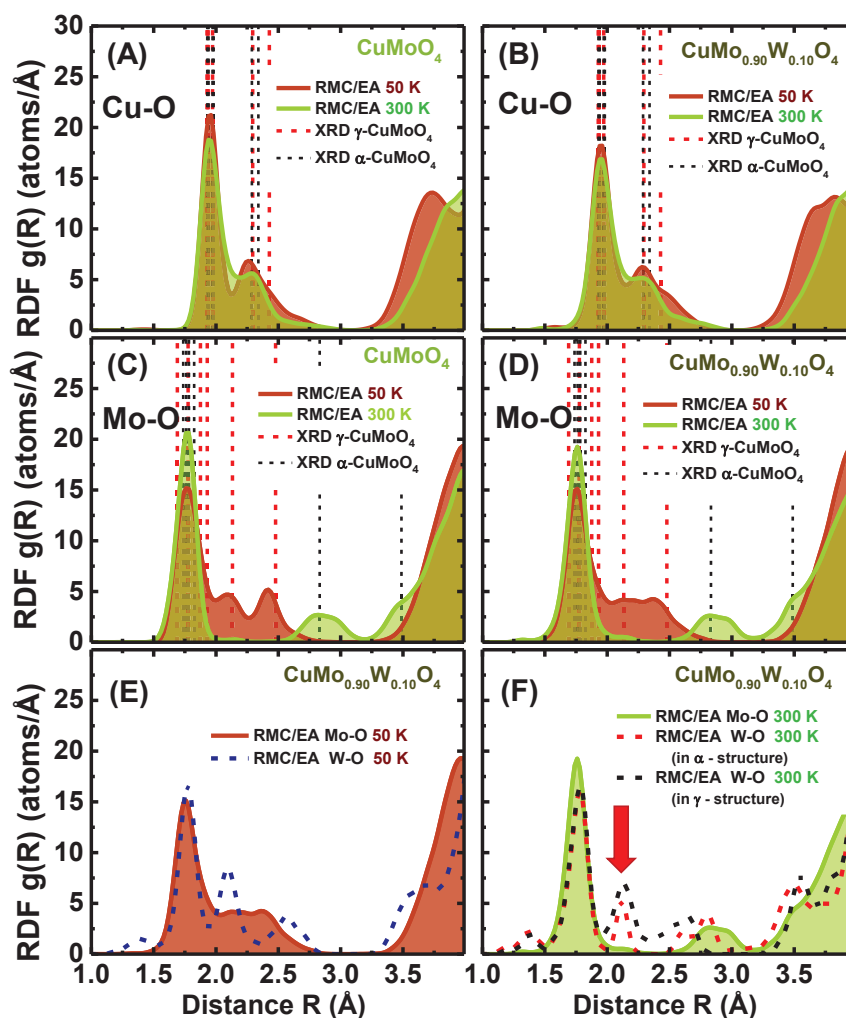
Figure 5: Radial distribution functions for Cu–O, Mo–O, W–O atom pairs in CuMoO$_4$ (A,C) and CuMo$_{0.90}$W$_{0.10}$O$_4$ (B,D,E,F), calculated from the atom coordinates of the RMC models. Dashed vertical lines show interatomic distances according to diffraction data (Wiesmann et al. (1997)). Vertical arrow in (F) indicates a group of oxygen atoms which does not exist in the tetrahedral coordination.

14